A microscopic model for the behavior of nanostructured organic photovoltaic devices

R. A. Marsh, C. Groves, and N. C. Greenham

Citation: Journal of Applied Physics **101**, 083509 (2007); doi: 10.1063/1.2718865
View online: http://dx.doi.org/10.1063/1.2718865
View Table of Contents: http://scitation.aip.org/content/aip/journal/jap/101/8?ver=pdfcov
Published by the AIP Publishing

A microscopic model for the behavior of nanostructured organic photovoltaic devices

R. A. Marsh,[a] C. Groves, and N. C. Greenham
Cavendish Laboratory, J. J. Thomson Avenue, Cambridge CB3 0HE, United Kingdom

(Received 15 December 2006; accepted 14 February 2007; published online 20 April 2007)

We present a Monte Carlo model of carrier separation and recombination in nanostructured organic photovoltaic (OPV) devices which takes into account all electrostatic interactions, energetic disorder, and polaronic effects. This permits a detailed analysis of the strong morphology dependence of carrier collection efficiency. We find that performance is determined both by the orientation of the heterojunction relative to the external electric field as well as by carrier confinement due to polymer intermixing. The model predicts that an idealized interdigitated structure could achieve overall efficiencies twice as high as blends. The model also reproduces the weakly sublinear intensity dependence of short-circuit photocurrent (I_{SC}) seen in experiment. We show that this is not the result of space-charge effects but of bimolecular recombination. Disconnected islands of polymer in coarser blends result in bimolecular recombination even at low intensities and should therefore be minimized. By including a microscopic description of dark injection, the model can describe the full current-voltage (J-V) characteristics of different OPV structures. We examine the effect of morphology, intensity, mobility, and recombination rate on key parameters such as short-circuit current, open-circuit voltage (V_{OC}), and fill factor (FF). The model reproduces the intensity-dependent contribution to V_{OC} in a bilayer above that of a blend observed in experiment. We find that performance in both bilayers and blends is very sensitive to the recombination rate across the heterojunction. The model also predicts a striking dependence of performance on mobility. Indeed it is shown that a tenfold increase in mobility dramatically improves I_{SC} and FF and doubles the maximum power output in a bilayer device. As well as informing routes for improving device performance, the model also offers an improved microscopic understanding of OPV operation. © *2007 American Institute of Physics*. [DOI: 10.1063/1.2718865]

I. INTRODUCTION

Organic semiconductors offer a wide variety of applications, including displays[1,2] and plastic transistor circuits.[3–6] They also offer the potential to reduce significantly the cost of photovoltaic energy[7–9] due to solution processing and continuous deposition techniques. However, despite improvements in materials[10] and device design,[11–13] power conversion efficiencies remain prohibitively low for commercial exploitation (1.7% in polymer blends[14] and 4.4% in polymer: fullerene systems[15]). Therefore, further improvements are required before this potential can be realized. Much research is currently focused on understanding the efficiency-limiting mechanisms in organic photovoltaic (OPV) devices and how they may be minimized.

Experimentally, it is difficult to differentiate between the microscopic processes which determine overall OPV performance. Geminate recombination, bimolecular recombination, and space-charge effects can all play a role,[16] and the exact effect of morphology on each of these processes is still the subject of debate.[17] Further research is required to identify the exact physical origin of the full current-voltage curve, in particular the factors which determine the open-circuit voltage[18] and fill factor.[19]

Computational modeling offers a way of investigating these issues and informing ongoing experimental work. The majority of modeling thus far has employed a continuum approach.[20–22] While computationally efficient, this is unable to describe carrier interactions accurately and reduces morphological effects to bulk parameters. A proper inclusion of these effects requires a microscopic approach, which is computationally much more demanding, and hence only rarely adopted.[23–25] The most complete microscopic model of OPV operation so far[26] examines the effect of morphology on short-circuit behavior.

We present here a more complete microscopic model which includes polaronic effects, energetic disorder, and a full description of electrostatic interactions between carriers and with the electrodes. Crucially, modeling dark injection at the electrodes permits an investigation of the full J-V curve. The resulting model is used to analyze the effect of morphology, mobility, and incident light intensity on carrier collection efficiency, open-circuit voltage, and fill factor.

II. THE MODEL

A. Morphology

In order to investigate the effects of morphology on device performance, we require a series of blends. Rather than attempt an accurate description of spin coating of polymers, here we adopt the cellular automata approach used by Peumans *et al.*[27] The blend is discretized into a Cartesian

[a]Electronic mail: ram47@cam.ac.uk

lattice and initialized in a 1:1 ratio of each semiconductor, with a random spatial distribution. Phase separation is ensured by the appropriate choice of interfacial energies between materials A and B, denoted as E_{AA}, E_{BB}, and E_{AB},

$$(2E_{AB} - E_{AA} - E_{BB}) > 0. \quad (1)$$

Blend coarsening takes place through pairwise probabilistic swaps between neighboring lattice sites. Swapping rates are weighted by their corresponding Boltzmann factors in order to satisfy the condition of detailed balance. This method was shown by Peumans *et al.* to give a reasonable description of the structures produced by molecular demixing and is adequate for the purpose of investigating morphological effects in polymer blend devices. We can obtain a measure of the characteristic feature size a in these blends from the ratio of interfacial area A to total blend volume V,

$$a = \frac{3V}{A}. \quad (2)$$

B. Photovoltaic performance

We examine the factors which determine the balance between carrier separation and recombination, and hence carrier collection efficiency. We do not address exciton diffusion to the heterojunction here. In most photovoltaic cells based on blends, this is unlikely to be a performance-limiting step, as indicated by efficient photoluminescence (PL) quenching.[28] However, exciton diffusion will play a more important role in coarser blends and bilayer structures. Exciton diffusion can also be modeled using a dynamical Monte Carlo framework,[26] but here we choose to focus on charge separation and transport. In the model, pairs of carriers are created inside the device directly on either side of the heterojunction interface. Their hopping transition probabilities are calculated using Marcus rate expressions,[29] thus taking into account polaronic effects. Electrons may only hop between sites occupied by the electron accepting material, and similarly for holes. Energetic disorder in the materials is modeled using a Gaussian density of states.

Crucially, all electrostatic interactions in the device are included in the model. These include Coulombic repulsion between like charges, attraction between unlike charges, and image charge effects at each electrode. The sphere of influence of each carrier is taken as the thermal capture radius

$$r_{tc} = \frac{e^2}{4\pi\epsilon\epsilon_0 kT}. \quad (3)$$

Once generated, carriers move under the influence of these interactions, as well as the internal electric field. They may recombine either geminately or nongeminately (bimolecularly) across a heterojunction interface, or be extracted at one or other electrode.

The device is discretized into a lattice of hopping sites, within which carrier dynamics are simulated using a dynamical Monte Carlo (DMC) algorithm.[30] To make these simulations possible on a desktop personal computer (PC) we employ the first reaction method (FRM). The FRM is an approximation which reduces the number of calculations required by a factor equal to the number of competing processes in the model, which in this case represents several orders of magnitude. In a full DMC implementation, the probability of every allowed process is recalculated every time the system's configuration changes. In the FRM approach, this probability is calculated just once when that process is first enabled. This means that each carrier's next hop is not updated as other carriers move around it. However, this is expected to be a very reasonable approximation in the low carrier density regime, in which OPVs operate.

To confirm the validity of the FRM, we have compared it to a full DMC algorithm in which the behavior of all particles is updated after each carrier hop. The competition between carrier separation and recombination in the FRM and DMC models was examined by recording the probability distribution functions of the recombination and carrier escape times (defined as when the carriers have attained a separation that is greater than the thermal capture radius) for a single geminate pair in a bilayer. For brevity, these data are not shown, but the dynamical behavior of the carriers as predicted by both models is indistinguishable for a variety of electric field strengths, degrees of energetic disorder, and orientations of the heterointerface to the electric field. Furthermore, both models were used to predict the carrier collection efficiency for a bilayer device under short-circuit conditions at a variety of incident light intensities. In all cases, the carrier collection efficiencies predicted by the two models are indistinguishable. We can therefore be confident that the FRM approach does not compromise the model's description of carrier separation and recombination. For a more detailed analysis of DMC and FRM algorithms, see Lukkien *et al.*[31] and Nelson.[24]

The FRM approach is implemented here using a queue of allowed events, ordered by their corresponding time interval. During each iteration of the algorithm, the event at the front of the queue is executed, and any newly enabled events (e.g., further hopping, recombination, or extraction at the electrodes) are assigned time intervals. For each carrier, the event with the shortest time interval is selected and inserted into the queue at the appropriate place. The interval $\tau_{i\to j}$ for a given hopping event with initial state i and final state j is determined probabilistically,

$$\tau_{i\to j} = -\ln(X)/R_{i\to j}, \quad (4)$$

where X is a random number in the interval $[0,1]$ and $R_{i\to j}$ is the characteristic hopping rate. The hopping rate is calculated using Marcus theory, in order to take polaronic effects into account,

$$R_{i\to j} = \nu_{hop} \exp\left[-\frac{(E_j - E_i + E_r)^2}{4E_r k_B T}\right]. \quad (5)$$

E_i and E_j are the energies of hopping sites i and j, respectively, and E_r corresponds to twice the polaronic binding energy. The prefactor ν_{hop} is chosen to give a mobility of 10^{-4} cm^2 V^{-1} s^{-1} for isoenergetic material. Hopping is restricted to adjacent sites, whose energy is calculated by taking a Gaussian density of states of standard deviation σ. For each data point, device performance is averaged over 50 configurations of Gaussian disorder. The temperature is taken to

be 298 K, and simulations are performed on a lattice measuring $70\times35\times35$ nm^3, with a mesh size of 1 nm. The light absorption profile is taken to be linear across the device. Previous work suggests that modified light absorption profiles only have a small impact on performance.[26]

To permit a full treatment of the *J-V* performance of devices, dark current is modeled by thermionic injection of carriers from the electrodes. It has been shown that such an approach adequately describes dark injection in organic semiconductors.[35]

This process is integrated into the FRM algorithm by queuing up carrier injection events in the same way as hopping and recombination events. Each electrode is discretized into a two-dimensional grid of carrier-injecting sites. In the same way as the hopping algorithm, each electrode site injects carriers at time intervals determined by its characteristic injection rate. This rate is calculated using the same Marcus rate expression, and therefore depends on the energy levels of the electrode and the adjacent polymer site. The injection barriers at the anode and cathode are both taken to be 0.4 eV, and hopping parameters for injection are taken as for polymer transport. Carrier extraction from the polymer to the adjacent electrode is treated as a hopping event in exactly the same way.

Although Gaussian broadening is taken into account, it should be noted that the FRM algorithm precludes the inclusion of the effect of the local electric field on the initial injection step. This is because the injection of one carrier has a significant effect on the injection of subsequent carriers at the same or neighboring sites, which would require immediate recalculation of the associated hopping times. To avoid this problem, we make the further approximation that the initial hopping rate is determined solely by the energy barrier between metal and organic, taking into account the Gaussian density of states, but neglecting the local electric field. Subsequent carrier motion through the device takes full account of the local electric field. Since the carrier densities in OPV devices are small [see Fig. 3(d)], this is a negligible correction. To validate this approach, we performed simulations of carrier injection in a full DMC model, recalculating the probability of each injection event after every carrier hop and taking into account the local electric field. The results are identical to those obtained using the FRM.

Coulombic interactions with other carriers and the electrodes are modeled by calculating the modified potential in the region of each charge (up to the thermal capture radius). The inclusion of image charge effects ensures that the potential at each electrode is fixed. The potential monopole associated with each carrier within the device allows the model to describe band bending and space-charge effects. The built-in field at short circuit arises from the difference in electrode work functions $\Delta\phi$, which is dropped over the device of thickness d. Recombination events are allowed when opposite carriers occupy adjacent sites and are characterized by the recombination rate constant ν_r. For parameter values taken in the model, see Table I.

While experimentally reasonable, this parameter set is by no means uniquely valid. In particular, the recombination rate ν_r may vary by several orders of magnitude, depending on the materials chosen and the details of molecular interactions at the heterojunction. The effect of changing this parameter is investigated specifically in Sec. IV. The choice of hopping parameter values is best rationalized by measuring the effective bulk mobility it produces in pristine material, see Fig. 1. We find mobilities of reasonable magnitude, and we can reproduce the Poole-Frenkel-type electric field dependence characteristic of hopping in disordered materials such as semiconducting polymers. A fit of the form $\mu(E)=\mu_0\times e^{\gamma\sqrt{E}}$ yields $\mu_0=1.0\times10^{-5}$ cm^2 V^{-1} s^{-1} and $\gamma=1.6\times10^{-4}$ m$^{1/2}$ V$^{-1/2}$.

TABLE I. Parameters used in the model.

ϵ	4
ν_r	5×10^5 s^{-1}
E_r	3×10^{-20} J
ν_{hop}	6.76×10^{11} s^{-1}
σ	1×10^{-20} J
$\Delta\phi$	1.2 V
d	70 nm

III. SHORT-CIRCUIT PERFORMANCE

Simulations of short-circuit behavior were performed for a set of morphologies, including a bilayer, blends of differing coarseness, and an idealized interdigitated morphology, see Fig. 2. It is found that carrier collection efficiency (η_{CC}) depends very strongly on morphology, see Fig. 3(a). Coarsening of the blend morphology leads to an increase in η_{CC}, consistent with the results reported by Watkins *et al.*[26] The high η_{CC} displayed by the bilayer is expected, but in practice does not lead to high external quantum efficiencies (EQEs) because of poor exciton diffusion efficiency η_{ED}. However, the interdigitated structure may be expected to exhibit a η_{ED} similar to blends since its column width is comparable to the exciton diffusion length. A comparison of the η_{CC} values predicted suggests that such an ordered morphology could increase overall EQE dramatically, by up to a factor of 2 compared to blends.

The model permits an investigation of the competition between geminate and nongeminate (bimolecular) recombi-

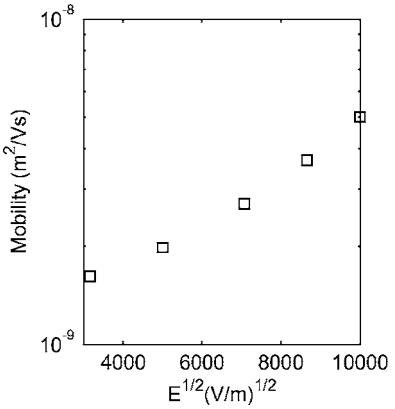

FIG. 1. Mobility as a function of electric field (E), generated using parameters from Table I.

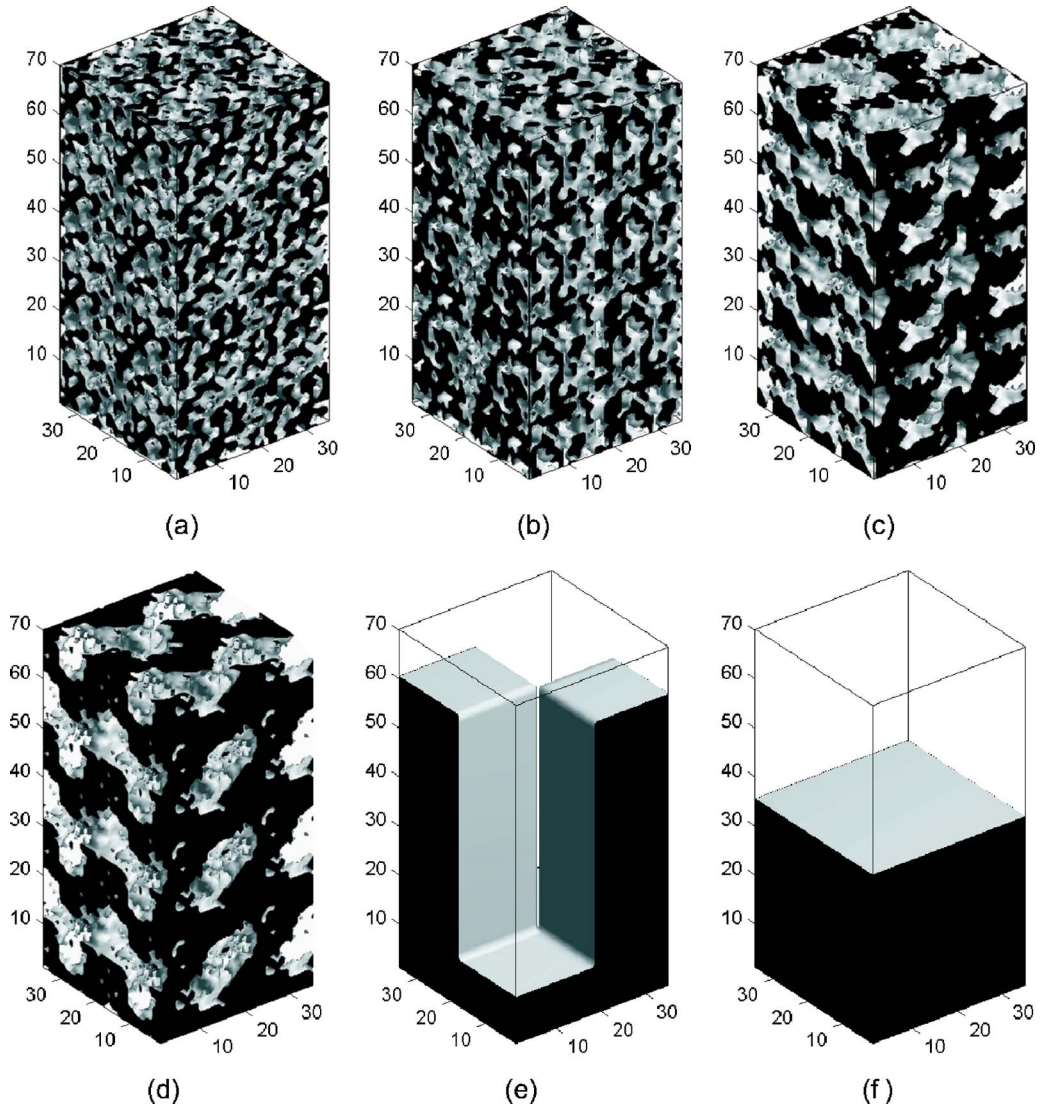

FIG. 2. (Color online) The different active layer morphologies investigated, with dimensions given in nm: [(a)–(d)] four blends of varying coarseness, with characteristic feature sizes of 2.5, 3.0, 4.3, and 5.8 nm, respectively; (e) an idealized interdigitated morphology, consisting of interpenetrating pure columns of polymer 17 nm in width with a 10 nm capping layer at top and bottom, analogous to the ordered structure investigated by Watkins *et al.*[26] and (f) a bilayer.

nations, defined by their probabilities η_{gr} and η_{or}, respectively. It is apparent from Figs. 3(b) and 3(c) that geminate recombination is dominant in all morphologies. This is consistent with experiment, where I_{SC} is found to scale almost linearly with light intensity.[32] The increased η_{gr} for the interdigitated structure compared to the bilayer illustrates the importance of the orientation of the heterojunction relative to the electric field. We can therefore partly assign the poorer performance of blend devices to the fact that the heterojunctions are randomly aligned with respect to the electric field. Additionally, since there is also significant variation in η_{gr} within the range of blends modeled, we may identify impeded carrier motion during the initial separation process as a second effect leading to enhanced geminate recombination.

Varying light intensity permits an investigation of space-charge and bimolecular effects. Since this model is concerned with carrier collection, a comparison with solar intensities requires knowledge of light absorption efficiency (η_A) and exciton diffusion efficiencies (η_{ED}). These factors will depend on the particular device, but here we adopt a simple estimate, $\eta_A \times \eta_{ED}=0.25$ under AM1.5 conditions. The weak decrease in η_{CC} with increasing intensity seen in experiment[32] is reproduced by the model. However, Fig. 3(b) illustrates that geminate recombination is unchanged, indicating that the local electric field is also unaffected. Hence we may conclude that space-charge effects are not responsible for the behavior we observe. (Note that we have chosen equal electron and hole mobilities, and that space-charge effects are likely to play a more prominent role when there is a mismatch in electron and hole mobilities.[33,34]) Figures 3(c) and 3(d) show that, in our simulation, the intensity dependence of η_{CC} results from bimolecular recombination. Moreover, this exhibits a largely quadratic dependence on intensity, as would be expected. The linear contribution apparent for the two coarsest blends may be assigned to islands topologically disconnected from the electrodes, which in order of increasing feature size, constitute 0.6%, 0.7%, 1.3%, and 1.8% by volume of the blends modeled. Any carriers generated on these islands serve as recombination sites, producing

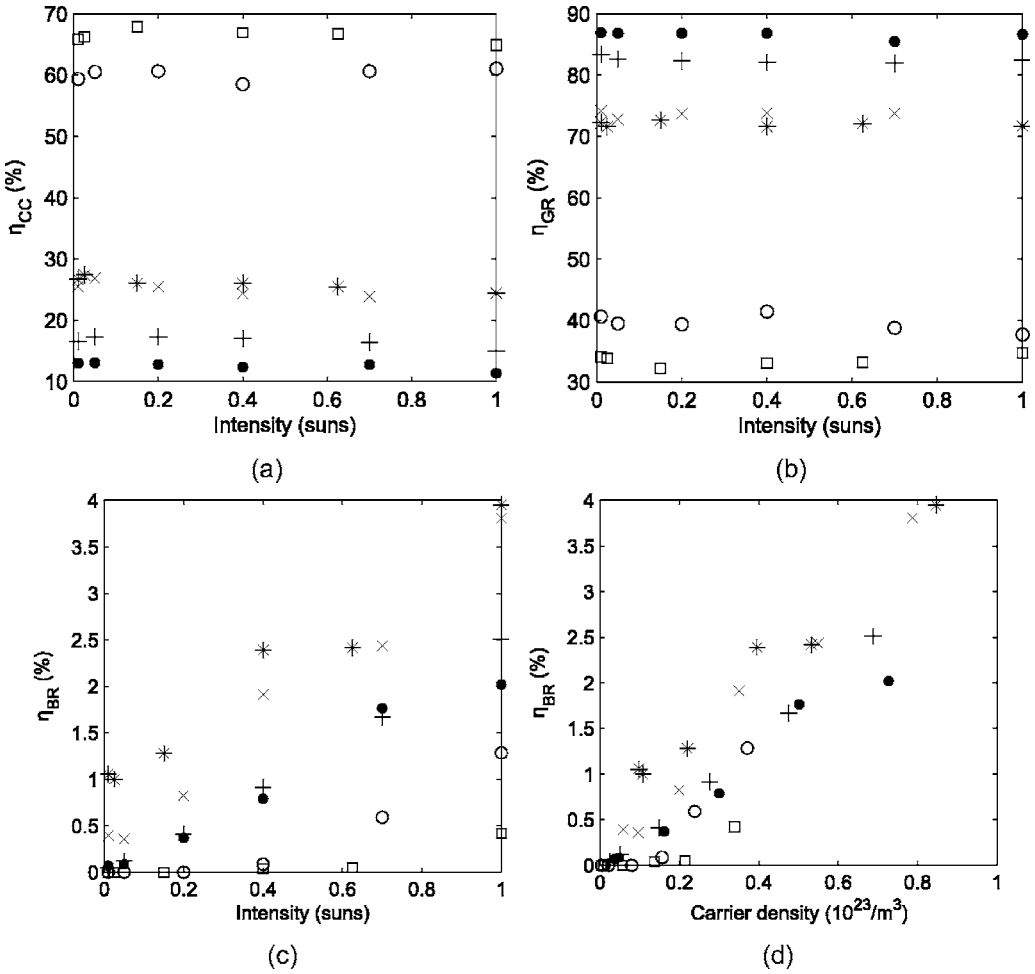

FIG. 3. Short-circuit behavior as a function of intensity for a bilayer (squares), an interdigitated structure (circles), and blends of feature sizes of 5.8 nm (asterisks), 4.3 nm (×), 3.0 nm (+), and 2.5 nm (dots). The subfigures illustrate (a) carrier collection efficiency, (b) geminate recombination efficiency, and [(c) and (d)] bimolecular recombination efficiency.

a monomolecular contribution to η_{or}. Hence we may identify disconnected islands as a source of loss in blend morphologies even at low intensities.

IV. CURRENT-VOLTAGE CHARACTERISTICS

The model is employed to investigate the effect of morphology, intensity, mobility, and recombination rate on the full *J-V* curve. Detailed results are illustrated in Fig. 4 and key performance parameters are summarized in Table II.

At short circuit it was found that carrier separation is much more efficient in a bilayer than in blends (see Sec. III). We find that this is still the case towards open circuit, as indicated by an increased fill factor (FF). Open circuit in the blend corresponds approximately to flatband conditions. This is because, in the absence of an internal electric field, carriers diffuse in a direction determined by the orientation of the heterojunction. It is important to note here that diffusion is effectively the result of a biased random walk, owing to the volume excluded by the opposite polymer type. In the blend these heterojunctions are oriented at random with respect to the electrodes, and so produce no net photocurrent at zero internal field. In the case of a bilayer device, every heterojunction is aligned so as to direct carriers to the appropriate electrode. This results in a nonzero net current at flatband conditions. To reach open-circuit conditions, an internal field is required to oppose this carrier motion, which explains the additional contribution to V_{OC} in the bilayer device.[21]

The superior fill factor of the bilayer device is not the result of more efficient charge separation. Geminate recombination exhibits a linear voltage dependence in both cases, which would produce a fill factor of 0.25 in the absence of bimolecular recombination. The difference is that, a flatband conditions, geminate recombination in the blend is almost 100% whereas in the bilayer it is only 80%. If extrapolated, geminate recombination in the bilayer would only reach 100% at around 1.7 V. However, beyond flatband conditions, the bias acts to confine charges at the heterojunction, resulting in increased local charge densities and hence bimolecular recombination. It is this mechanism which limits V_{OC} to 1.4 V and determines the shape of the *J-V* curve around V_{OC}. This indicates that V_{OC} is strongly affected by the charge density at the bilayer interface.

To investigate this effect further, we model the *J-V* characteristics of a bilayer over three orders of magnitude of light intensity. At 0.1 and 1 sun, the short-circuit behavior and fill factor are relatively unchanged. Consistent with our findings at short circuit, bimolecular recombination increases slightly, but geminate recombination remains the dominant loss

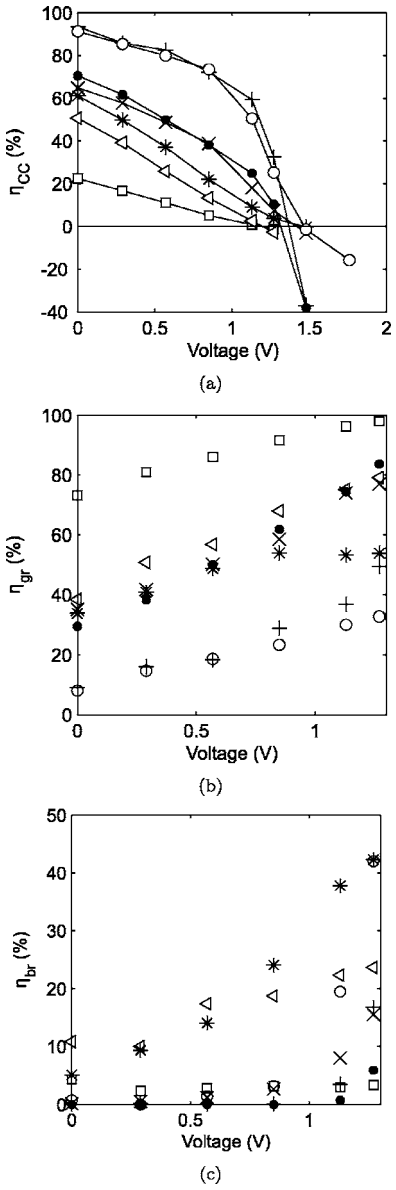

FIG. 4. Voltage-dependent behavior of a blend device, with characteristic feature size of 4.8 nm, at 1 sun (squares); a bilayer at 0.1 sun (dots), 1 sun (×), and 10 sun (asterisks); a bilayer at 1 sun with ten times the mobility (+); and a bilayer (circles) and a blend (triangles) with one tenth the recombination rate. The subfigures illustrate (a) carrier collection efficiency, (b) geminate recombination efficiency, and (c) bimolecular recombination efficiency.

mechanism. There is no evidence of space-charge effects even towards open-circuit conditions. However, the extra contribution to V_{OC} increases with intensity, as found in experiment.[36] The magnitude of this increase, 0.09 ± 0.03 V/decade, is consistent with the result predicted by a theoretical analysis based on superposition of dark and light current (0.06 V/decade).[21] At the highest intensity simulated, 10 sun, the behavior of the bilayer is markedly different. Bimolecular recombination is dramatically higher even at short circuit. Towards open circuit, carrier densities at the interface are so high that bimolecular recombination competes with geminate recombination. This behavior produces a pronounced drop in the fill factor. It also accounts for the smaller increase observed in V_{OC} between 1 and 10 sun.

In order to explore the effect of mobility on device performance, we compare the behavior of a bilayer at 1 sun where $\mu_0 = 1 \times 10^{-5}$ cm^2 V^{-1} s^{-1}, as above, with the case where $\mu_0 = 1 \times 10^{-4}$ cm^2 V^{-1} s^{-1}. We find that this tenfold increase in mobility produces a striking improvement in *J-V* characteristics. Carrier separation at short circuit approaches 100% efficiency. Moreover, it begins to saturate at a smaller internal field, producing a higher fill factor of 51%. Notably, the open-circuit voltage is unaffected. The overall effect of improved mobility is that carrier separation is much improved, and the maximum power, which is proportional to $\eta_{CC} \times V_{OC} \times \mathrm{FF}$, is doubled.

These results demonstrate clearly that device performance is strongly influenced by the direct competition between initial carrier separation and recombination. To investigate this further, we reduce the recombination rate by a factor of 10 in both blend and bilayer. In the blend, this simply rescales the entire *J-V* curve: FF and V_{OC} are unchanged. While the shape of the *J-V* curve remains the same (linear), the magnitude of the photocurrent, and hence the maximum power output, is increased by a factor of 2.5. The significantly enhanced role of bimolecular recombination in this case indicates that poor transport through the blend becomes a significant loss mechanism when initial carrier separation is highly efficient. This is analogous to the regime in which polymer:fullerene cells operate.[37,38] Such efficient carrier separation also explains the superior fill factors these devices often exhibit.

Suppressed recombination in the bilayer device produces a more pronounced change in performance. As in the blend, geminate recombination is reduced dramatically. However, the effect here is to increase not just I_{SC}, but also FF and V_{OC}. We note that the *J-V* characteristics are very similar to the case where the mobility is increased tenfold. These two *J-V* curves coincide up to voltages approaching open circuit. Here, suppressed recombination reduces dark current, since it can only flow via bimolecular recombination in the bilayer device. The result is a greater increase in V_{OC} than in the increased mobility case. The maximum power output is doubled.

Our model allows us to test at a microscopic level some of the theoretical descriptions of charge separation used in continuum models of photovoltaic devices. The observation that carrier separation efficiency is strongly dependent on mobility and on the recombination rate at the heterojunction shows that simple Onsager theory[39] (which neglects energetic disorder and assumes an infinite recombination rate at the origin) is insufficient. The extension of Onsager theory by Braun,[40] which takes into account the competition between separation and finite-speed recombination gives a better match to our microscopic model, and has been successfully used to produce a refined continuum description of OPV devices.[34]

However, our results show that to understand the behavior of OPV devices, bulk parameters alone are not sufficient, even when Braun's model is invoked. The continuum approach of describing morphological dependence through effective bulk mobilities cannot explain the dependence of efficiency on blend coarseness seen in our model. Restricted

TABLE II. Key results for different morphologies, intensities, and mobilities. The blend has a characteristic feature size of 4.3 nm. μ has a value of 10^{-5} $cm^2/V\,s$ at zero electric field, see Fig. 1.

Morphology	Intensity (sun)	ν_r (s^{-1})	Mobility	η_{CC}	V_{OC} (V)	FF
Blend	1	5×10^5	μ	22% ±1%	1.18±0.01	24% ±1%
Bilayer	0.1	1×10^5	μ	70% ±2%	1.32±0.02	34% ±1%
Bilayer	1	5×10^5	μ	65% ±4%	1.41±0.02	36% ±2%
Bilayer	10	5×10^5	μ	61% ±1%	1.46±0.01	24% ±0.5%
Bilayer	1	5×10^5	10μ	94% ±1%	1.39±0.02	51% ±1%
Blend	1	5×10^4	μ	51% ±2%	1.20±0.01	24% ±1%
Bilayer	1	5×10^4	μ	91% ±5%	1.46±0.02	47% ±2%

motion of carriers in blends after initial separation of the geminate pair impairs efficiency; however, our simulations of carrier transport through the devices indicate that the effective bulk mobility is barely affected by blend coarseness, and therefore cannot be invoked to explain this effect.

V. CONCLUSIONS

We have developed a comprehensive microscopic model of carrier separation and recombination in OPV devices, which includes polaronic effects, energetic disorder, all electrostatic interactions, as well as dark injection. By analyzing carrier dynamics in different structures and under different light intensities and biases, this permits an improved theoretical understanding of experimental observations. These include the weak intensity dependence of carrier collection efficiency, which we attribute not to space-charge effects but to bimolecular recombination. The model also explains the additional open-circuit voltage in bilayers compared to blends, which is itself intensity dependent.

Furthermore, the model may be used to evaluate different strategies for improving device performance. The model predicts that an idealized interdigitated morphology could double the carrier collection efficiency achieved in a blend. Our results also suggest that the maximum power output is extremely sensitive both to the geminate recombination rate across the heterojunction and to carrier mobility. Our microscopic model identifies that the efficiency depends on morphology in ways that cannot be explained by continuum approaches based on bulk parameters.

ACKNOWLEDGMENTS

The authors are grateful to Dr. A. B. Walker for helpful discussions. This work was supported by the EU Integrated Project NAIMO (No. NMP4-CT-2004-500355). One of the authors (R.A.M.) thanks the George and Lilian Schiff Foundation for financial support.

[1] J. H. Burroughes, D. D. C. Bradley, A. R. Brown, R. N. Marks, K. Mackay, R. H. Friend, P. L. Burns, and A. B. Holmes, Nature (London) **347**, 539 (1990).
[2] J.-S. Kim and R. H. Friend, Appl. Phys. Lett. **87**, 023506 (2005).
[3] R. F. Service, Science **278**, 383 (1997).
[4] C. J. Drury, C. M. J. Mutsaers, C. M. Hart, M. Matters, and D. M. de Leeuw, Appl. Phys. Lett. **73**, 108 (1998).
[5] J. A. Rogers, Z. N. Bao, A. Makhija, and P. Braun, Adv. Mater. (Weinheim, Ger.) **11**, 741 (1999).
[6] H. Sirringhaus, N. Tessler, and R. H. Friend, Science **280**, 1741 (1998).
[7] N. S. Sariciftci, D. Braun, C. Zhang, V. I. Srdanov, A. J. Heeger, G. Stucky, and F. Wudl, Appl. Phys. Lett. **62**, 585 (1993).
[8] G. Yu, J. Gao, J. C. Hummelen, F. Wudl, and A. J. Heeger, Science **270**, 1789 (1995).
[9] M. Granstrom, K. Petritsch, A. C. Arias, A. Lux, M. R. Andersson, and R. H. Friend, Nature (London) **395**, 257 (1998).
[10] C. J. Brabec, C. Winder, M. C. Scharber, N. S. Sariciftci, J. C. Hummelen, M. Svensson, and M. R. Andersson, J. Chem. Phys. **115**, 7235 (2001).
[11] G. Yu and A. J. Heeger, J. Appl. Phys. **78**, 4510 (1995).
[12] S. E. Shaheen, C. J. Brabec, N. S. Sariciftci, F. Padinger, T. Fromherz, and J. C. Hummelen, Appl. Phys. Lett. **78**, 841 (2001).
[13] J. J. M. Halls, C. A. Walsh, N. C. Greenham, E. A. Marseglia, R. H. Friend, S. C. Moratti, and A. B. Holmes, Nature (London) **376**, 498 (1995).
[14] T. Kietzke, H. H. Horhold, and D. Neher, Chem. Mater. **17**, 6532 (2005).
[15] Y. Kim, S. Cook, S. M. Tuladhar, S. A. Choulis, J. Nelson, J. R. Durrant, D. D. C. Bradley, M. Giles, I. McCulloch, C. S. Ha, and M. Ree, Nat. Mater. **5**, 197 (2006).
[16] L. J. A. Koster, V. D. Mihailetchi, H. Xie, and P. W. M. Blom, Appl. Phys. Lett. **87**, 203502 (2005).
[17] H. J. Snaith, A. C. Arias, A. C. Morteani, C. Silva, and R. H. Friend, Nano Lett. **2**, 1353 (2002).
[18] L. J. A. Koster, V. D. Mihailetchi, R. Ramaker, and P. W. M. Blom, Appl. Phys. Lett. **86**, 123509 (2005).
[19] V. Djara and J. C. Bernde, Thin Solid Films **493**, 273 (2005).
[20] H. H. P. Gommans, M. Kemerink, J. M. Kramer, and R. A. J. Janssen, Appl. Phys. Lett. **87**, 122104 (2005).
[21] J. A. Barker, C. M. Ramsdale, and N. C. Greenham, Phys. Rev. B **67**, 075205 (2003).
[22] C. M. Martin, V. M. Burlakov, and H. E. Assender, Sol. Energy Mater. Sol. Cells **90**, 900 (2006).
[23] P. Peumans and S. R. Forrest, Chem. Phys. Lett. **398**, 27 (2004).
[24] J. Nelson, Phys. Rev. B **67**, 155209 (2003).
[25] T. Offermans, S. C. J. Meskers, and R. A. J. Janssen, Chem. Phys. **308**, 125 (2005).
[26] P. K. Watkins, A. B. Walker, and G. L. B. Verschoor, Nano Lett. **5**, 1814 (2005).
[27] P. Peumans, S. Uchida, and S. R. Forrest, Nature (London) **425**, 158 (2003).
[28] C. Im, E. V. Emelianova, and H. Bässler, J. Chem. Phys. **117**, 1395 (2002).
[29] R. A. Marcus, Rev. Mod. Phys. **65**, 599 (1993).
[30] D. P. Landau and K. Binder, *Guide to Monte Carlo Simulations in Statistical Physics* (Cambridge University Press, Cambridge, 2000).
[31] J. J. Lukkien, J. P. L. Segersa, P. A. J. Hilbers, R. J. Gelten, and A. P. J. Jansen, Phys. Rev. E **58**, 2598 (1998).
[32] P. Schilinsky, C. Waldauf, and C. J. Brabec, Appl. Phys. Lett. **81**, 3885 (2002).
[33] N. Tessler and N. Rappaport, Appl. Phys. Lett. **89**, 013504 (2006).
[34] L. J. A. Koster, E. C. P. Smits, V. D. Mihailetchi, and P. W. M. Blom, Phys. Rev. B **72**, 085205 (2005).
[35] U. Wolf, V. I. Arkhipov, and H. Bässler, Phys. Rev. B **59**, 7507 (1999).
[36] C. M. Ramsdale, J. A. Barker, A. C. Arias, J. D. MacKenzie, R. H. Friend, and N. C. Greenham, J. Appl. Phys. **92**, 4266 (2002).
[37] J. G. Muller, J. M. Lupton, J. Feldmann, U. Lemmer, M. Scharber, N. S. Sariciftci, C. J. Brabec, and U. Scherf, Phys. Rev. B **72**, 195208 (2005).
[38] P. Schilinsky, C. Waldauf, and C. J. Brabec, Appl. Phys. Lett. **81**, 3885 (2002).
[39] L. Onsager, Phys. Rev. **54**, 554 (1938).
[40] C. L. Braun, J. Chem. Phys. **80**, 4157 (1984).